Electronic properties of bulk γ-Al_2O_3

E. Menéndez-Proupin and G. Gutiérrez*
Departamento de Física, Facultad de Ciencias, Universidad de Chile, Casilla 653, Santiago, Chile
(Received 6 December 2004; revised manuscript received 5 April 2005; published 14 July 2005)

The electronic structure of bulk γ-alumina is investigated using Density Functional Theory. Recent theoretical structures, including occupation of nonspinel positions, are used as starting point for energy minimization, allowing for relaxation of the cell shape and the ionic positions. A comparison of simulated diffraction patterns of the present and recent theoretical and experimental structural models is presented. The electronic structure is described in terms of band structure, density of states, charge density, electron localization function, and ionic charges. The valence band density of states of γ-alumina is similar to α- and κ-alumina, although a smaller bandgap is found. It is shown that γ-alumina ionicity is similar to other alumina phases, with a high localization of the electrons at oxygen atoms. The smaller bandgap of γ-alumina is attributed to the structural disorder.

DOI: 10.1103/PhysRevB.72.035116 PACS number(s): 71.20.Nr, 71.20.Ps, 81.05.Je

I. INTRODUCTION

γ-Al_2O_3 is a form of aluminum oxide (alumina) that is obtained by thermal decomposition, at $T \sim 800$ K, of boehmite (AlOOH), a major constituent in many bauxites.[1] γ-alumina is a transition form, and upon further heating undergoes a sequence of phase transformations up to corundum (α-alumina). γ-Al_2O_3 presents a porous structure at nanometer scale, which makes it useful for a variety of industrial processes, such as catalysis,[2] structural composites in spacecraft, and abrasive and thermal coatings.[3]

As other transition aluminas, this material presents a low degree of crystallinity, due to which its structure is not well known. Early x-ray studies established that γ-alumina is a kind of defect spinel structure[4] with the space group $Fd\bar{3}m$.[5] Frequently, the structure has been reported as tetragonal, considered as contraction of the cubic lattice along one of the cubic crystallographic directions, but only recently a tetragonal space group, $I4_1/amd$, has been proposed (see Ref. 3 and references therein). The presence of the tetragonal distortion is related to the preparation history and the precursor mineral. The O ions form a cubic closed packed lattice (inherited from its precursor, the boehmite mineral), while the Al cations occupy interstitial sites with both octahedral and tetrahedral coordination, leaving unoccupied a fraction of the available sites. In the spinel structure, the interstitial sites occupied by Al cations are restricted to the 8*a* (tetrahedral) and 16*d* (octahedral) Wyckoff positions. However, to satisfy the Al_2O_3 stoichiometry some Al vacancies must be introduced. This is the origin of the historical formula for the conventional cubic cell $\square_{2(2/3)}Al_{21(1/3)}O_{32}$, where $\square$ stands for a vacancy at the spinel sites. The distribution of the vacancies has been the subject of great controversy.[6] Some studies indicate that the vacancies are at tetrahedral sites, others at octahedral, and others show different proportions of tetrahedral and octahedral vacancies.

Recent models based on neutron scattering place Al cations at nonspinel sites, such as 32*e* and 16*c* of the $Fd\bar{3}m$ space group,[3,5] and 8*c* of the $I4_1/amd$ space group.[3,7] In these models the available sites outnumber the amount of cations necessary to satisfy the Al_2O_3 stoichiometry. Hence, fractional site occupation factors are introduced as fitting parameters. These fractional occupation factors mean that the structure is not strictly periodic, each conventional cell has occupied a different set of the available sites, the average of which is the Rietveld refined structure. Another possibility is that space group has lower symmetry than $Fd\bar{3}m$, so that the multiplicity of the Wyckoff sites is smaller and the site occupation factors are 1. This is the kind of structure that has been obtained by theoretical methods in recent years.[6,8–12] The main difficulty with the experimentally obtained structures is the fractional number of $21\left(\frac{1}{3}\right)$ Al cations in the conventional cell of the spinel structure. In order to obtain a unit cell with integer number of atoms, a cell of 160 atoms is needed, with 96 O atoms, 64 Al atoms, and 8 cation vacancies. The large number of configurations has handicapped the use of first-principles methods, and the tiny differences in energy among the configurations have made unreliable the use of classical force methods, which so far have provided contradictory results.[13–15] An elegant alternative consists in the following transformation of the vacancy-free structure. Consider its primitive cell, which has the formula Al_6O_8 (the conventional cell contains four lattice points). Taking any unit cell containing three lattice points and eliminating two Al cations, a cell with the formula $Al_{16}O_{24}$ and two vacant spinel sites is obtained. These cells have the required stoichiometry 2:3 and an integer number of atoms. Let us notice that after establishing the vacancies, the space group has lower symmetry than $Fd\bar{3}m$. The number of nonequivalent combinations of the vacant sites turns out to be 14,[6] which is a number of configurations small enough to be afforded by *ab initio* calculations. Recent *ab initio* calculations based on this approach[6,8–10] have led to theoretical structures that allow a detailed analysis of the position of the vacancies. All these reports conclude that the minimum energy structures contain only octahedral Al vacancies at positions that are most far away from each other. These *ab initio* structures have been used to calculate electronic,[10] optical,[16] and surface properties.[2,10] Two other issues deserve some comment. One is the content of hydrogen. Sohlberg *et al.*[11,12] proposed

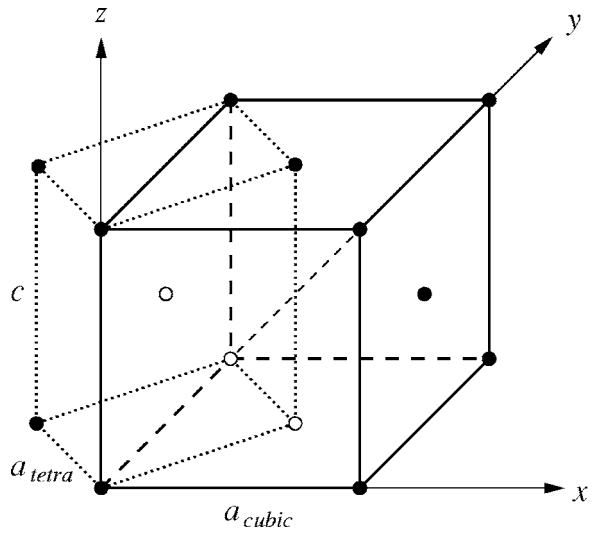

FIG. 1. The relation between the conventional cells of the groups $Fd\bar{3}m$ (solid line) and $I4_1/amd$ (dotted line).

a sequence of hydrogenated compounds $H_{3m}Al_{2-m}O_3$ to describe the transition from boehmite (AlOOH) to $Al_2O_3+H_2O$. In this sequence, the minimal energy corresponds to $m=1/8$ (with integer subscripts: HAl_5O_8) and was identified with the most probable γ-alumina structure. However, Wolverton and Haas[17] calculated that HAl_5O_8 is thermodynamically unstable against $AlOOH+2Al_2O_3$. Recent experimental data[3,5] suggest that hydrogen is not a structural component of crystalline γ-alumina, but is stored at amorphous regions.[18]

Most of the theoretical models up to now consider Al cations restricted to spinel positions. This restriction was removed in a recent computational study by Paglia *et al.*[19] By combining empirical interatomic potentials and density functional theory[20] (DFT), they explored a huge number of structures where the Al cations are distributed at 8*a*, 16*c*, and 16*d* positions, restricting the relative site occupancies to the proportion obtained from Rietveld refinement of neutron scattering data,[3,7] as well as the lattice parameters. The Al-Al repulsion due to the close proximity of 16*c* and 8*a* sites causes that during the relaxation some Al atoms migrate to other Wyckoff sites (mostly to 48*f*). In this way, Paglia *et al.* found theoretical minimum energy structures that achieve the best agreement with the experimental diffraction patterns. A representative structure has been detailed[19] to each of the space groups $Fd\bar{3}m$ and $I4_1/amd$. The relation between the conventional unit cells of these groups is shown in Fig. 1. The $I4_1/amd$ tetragonal cell (dotted lines) has half of the volume of the $Fd\bar{3}m$ cubic unit cell (solid lines), with $a_{cubic}=\sqrt{2}a_{tetra}$. The tetragonal distortion is obtained by making $c\neq a_{cubic}$. The experimental values reported for c/a_{cubic} are in the range 0.963–0.987.[3] The occupied Wyckoff positions and their relations in both space groups are summarized in Table I. Positions *a*, *b*, *c*, and *d* are completely equivalent in both groups, the multiplicity for $I4_1/amd$ being half of that for $Fd\bar{3}m$ due to the volume ratio of the conventional cells. When the symmetry is lowered, 48*f* and 32*e* sites become 8*e*+16*g* and 16*h*, respectively, but the opposite transformation is not true in general. For instance, in the Rietveld refined structure reported in Refs. 3 and 7, the O 16*h* positions are derived from the 32*e* positions of the cubic symmetry and allowed to relax with the constraints of the $I4_1/amd$ group. Going back to the $Fd\bar{3}m$, the tetragonal refined O positions do not correspond exactly to 32*e*, but within a certain tolerance. On the other hand, the 8*e* and 16*g* Al sites obtained in Ref. 19 do not correspond to any 48*f* site in $Fd\bar{3}m$.

TABLE I. The relation between the occupied Wyckoff positions in the structural models of γ-alumina according to the space groups $Fd\bar{3}m$ and $I4_1/amd$. Octahedral (o) and tetrahedral (t) coordination are specified. Bidirectional arrows indicate equivalence. Rightsided arrows indicate that the transformation from $I4_1/amd$ to $Fd\bar{3}m$ is conditioned by constraints in the coordinates.

	$Fd\bar{3}m$		$I4_1/amd$
Al(t)	8*a*	↔	4*a*
Al(t)	8*b*	↔	4*b*
Al(t)	48*f*	→	8*e*+16*g*
Al(o)	16*c*	↔	8*c*
Al(o)	16*d*	↔	8*d*
O	32*e*	→	16*h*

The computational models obtained by Paglia *et al.* are referred to 160-atom supercells. These supercells are $2\times1\times3$ and $1\times1\times3$ arrays of the conventional cell of the space groups $I4_1/amd$ and $Fd\bar{3}m$, respectively. These supercells have general symmetry *P*1, i.e., only translational symmetry. These unit cells must not be regarded as the *actual* structures, but as *representative* of a rather large number of structures that have very close energies. The ensemble of all the possible low energy structures is equivalent to the experimentally Rietveld refined structure with fractional site occupation factor, while the representative structures provide a basis for theoretical modeling without the inconvenient fractional site occupation factors.

Figure 2 shows simulated neutron diffraction powder patterns for theoretical[6,10] and experimental[3,5] structures. The structure of Ref. 6 was obtained from a spinel model, relaxing the atomic positions and the unit cell volume, but not the unit cell shape. Further relaxation allowing the cell shape to vary results in a slightly distorted structure, the powder pattern of which is presented in the figure. Notice that the pattern of the structure of Gutierrez *et al.*[6] has a rather good agreement with the fitted pattern by Zhou and Snyder, although, differences in the relative peak intensities are apparent. However, the small peak at 38° does not appear in the experimental data.[5] The model of Paglia *et al.*[3] achieves the best quantitative and qualitative agreement with the experiment and should be regarded as the reference for comparison. The DFT models with relaxed unit cell agree better with the model of Paglia *et al.* A particular point for a qualitative discussion is the splitting at 46°–47°. This splitting is caused by the tetragonal distortion. If this distortion is removed by making $c=\sqrt{2}a$ ($I4_1/amd$ notation), then the splitting be-

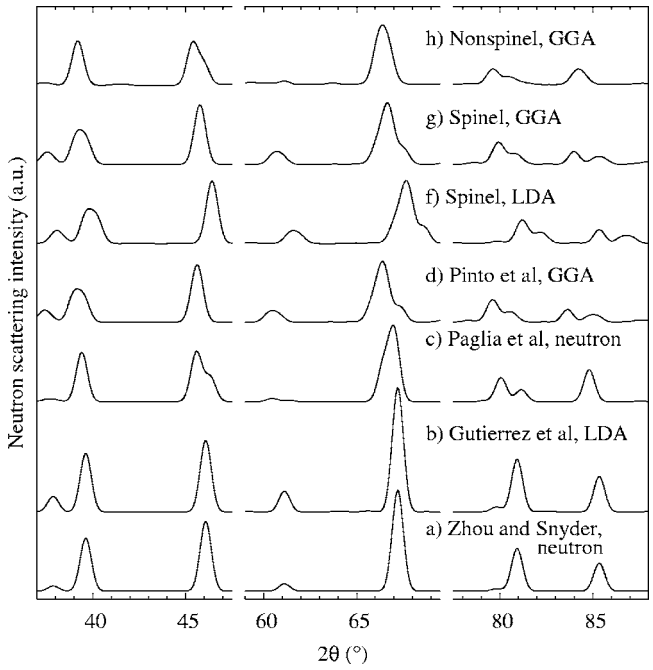

FIG. 2. The simulated neutron scattering spectra for different proposed models of γ-Al_2O_3 structure. The experimental structures were obtained by Rietveld refinement of neutron diffraction spectra. The theoretical structures have been obtained by relaxation of the atomic positions and cell shape [except (b)] to minimize the LDA or GGA energy. (a) Experimental nonspinel model (Ref. 5). (b) Theoretical spinel model (Ref. 6). (c) Experimental nonspinel model (Ref. 3). (d) Theoretical spinel model (Ref. 10). (f) Theoretical structure obtained in this work, allowing for cell relaxation of the structure (b) using LDA. (g) As (f), but using GGA. (h) Theoretical structure obtained in this work, allowing for cell relaxation of the nonspinel $Fd\bar{3}m$ model of Ref. 19. The spectra were generated with POWDERCELL 2.4 (Ref. 21), using $\lambda = 1.548$ Å, and a full-width at half-maximum FWHM=0.5°.

comes null. In the spinel-based DFT models there is a splitting of this peak, but it is smaller and is not appreciated in the figure (in fact, it is split in three peaks). There is also a qualitatively different splitting of the peaks at ~66° and 85°. Comparison of different spinel-based models reveals that the structure of Pinto *et al.*[10] and the structures obtained in this work by cell relaxation of the model of Gutierrez *et al.* are almost equal. The shift to higher angles in the diffraction peaks are caused by the well-known trend of the LDA to underestimate the equilibrium volume. The differences between both the spinel-based models and the Rietveld refined models is due to two factors. In the experimental structure, the distortion is a contraction of the cubic conventional unit cell along the *c* axis. In the DFT spinel models, the distortion of the conventional cubic cell can be described as a dilation along the *c* axis and a distortion of the angle γ from 90° to 89°. These different distortion modes are the cause of differences in the splitting of peaks at 46°, 66°, and 85°. On the other hand, the decrease of the intensities of the peaks at 38° and 61° is due to the transfer of Al cations from 16*d* to 16*c* sites.

Today with good structural models available, a study of the electronic properties can be done on sound foundations. In this report we present a detailed study of the electronic structure of γ-alumina, comparing the spinel model and the nonspinel model of Paglia *et al.*,[19] and other phases of alumina. We present the band diagram and the density of states (DOS), and explore the nature of the chemical bond in γ-alumina by analyzing the electron density, the electron localization function (ELF),[22–24] and estimating the charge transfer. In Sec. II, we explain the method of calculation. In Sec. III, we present the numerical results. Finally, we give our conclusions in Sec. IV. The spinel relaxed structure used in the calculations is detailed in the Appendix.

II. COMPUTATIONAL DETAILS

We have performed calculations of the electronic structure in the framework of DFT using the total-energy Vienna *ab initio* simulation program VASP.[25–28] We have chosen the exchange-correlation potential as approximated by the Perdew-Zunger[29] parametrization of the local density approximation (LDA) and the generalized gradient approximation (GGA) of Perdew and Wang 91. The valence electronic eigenfunctions are obtained from an expansion in plane waves, while the core electrons are replaced by the ultrasoft pseudopotentials (USPP) supplied in the VASP package. For all the GGA and selected LDA calculations we have employed projector augmented waves (PAW) instead of pseudopotentials. We have used a cutoff of 495 eV for the plane wave expansion, which guarantees a convergence of the total energy within 0.5 meV/atom. The calculations with the spinel model were performed using a unit cell of 40 atoms. To obtain a smooth density of states (DOS), the first Brillouin zone has been sampled with a Monkhorst-Pack $4\times4\times2$ *k* mesh centered at the Γ point. Unphysical oscillations of the density of states due to the finiteness of the *k*-space grid has been eliminated using a Fermi smearing of 0.2 eV. We have checked the accuracy of the mesh by comparison with a nonself-consistent calculation using a $15\times15\times9$ *k* mesh and the charge density extracted from the $4\times4\times2$ *k* mesh. To check the convergence of the selfconsistent total energy with the *k* mesh, we made single point calculations of the initial structure using larger meshes: noncentered $4\times4\times2$ *k* mesh [26 irreducible *k* points (IKP)], Γ-centered $4\times5\times3$ *k* mesh (24 IKP) and Γ-centered $6\times6\times3$ *k* mesh (34 IKP). These calculations allow us to estimate the error in 10^{-6} eV/atom, which is much less than the cutoff error. In order to estimate the error produced by the use of an oblique lattice [see unit cell in Fig. 7(b)] and fast Fourier transform mesh, we made a test calculation using an orthorhombic supercell with 160 atoms and a $2\times2\times1$ Monkhorst-Pack mesh, obtaining an energy difference smaller than 0.01 meV/atom with respect to the oblique lattice 40-atom unit cell. For the nonspinel model we used the $1\times1\times3$ supercell (160 atoms) of the $Fd\bar{3}m$ model,[19] and the *k* space was sampled using a Γ-only mesh and a $2\times2\times1$ Monkhorst-Pack mesh. A test calculation using a $3\times3\times1$ Monkhorst-Pack mesh shows a difference less than 0.003 and 2×10^{-5} eV/atom with respect to the Γ-only and the $2\times2\times1$ meshes, respectively. The total energy is 15 meV/atom higher than for the spinel structure.[45] As this structure was optimized with the lattice

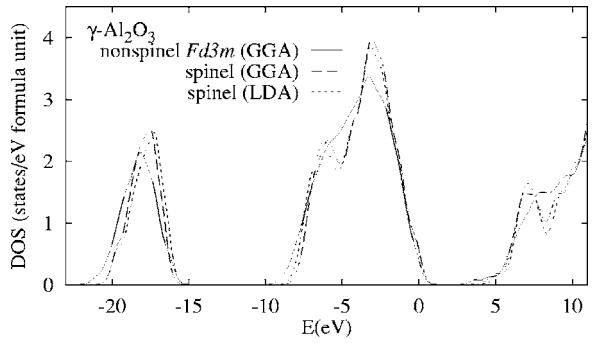

FIG. 3. The density of states of different structural models of γ-Al_2O_3: nonspinel model $Fd\bar{3}m$ of Ref. 19, and spinel model. A Fermi broadening of 0.2 eV is used.

parameters fixed to the experimental values,[19] we allowed the cell shape and atom positions to relax, obtaining a total energy that is still 5 meV/atom higher than for the spinel model, a volume increment of 3% (GGA) and a tetragonal distortion $c/a_{cubic}=0.987$.[46]

III. RESULTS

Figure 3 shows the DOS calculated for different structural models, including the spinel models (using both GGA and LDA) and the nonspinel model $Fd\bar{3}m$ of Paglia *et al.* (GGA). For the spinel structure, minimal differences occur due to the use of the LDA-USPP versus GGA-PAW methods. The nonspinel structure presents a smoother DOS: notice the fusion of the two peaks of the upper valence band, as well as the fusion of the two peaks in the lowest conduction band. It also shows a bandgap of 3.5 eV, smaller than the 3.8 and 4.2 eV of the optimized GGA and LDA spinel structures, respectively.

Figure 4 shows the total and the partial DOS of the nonspinel $Fd\bar{3}m$ model of γ-alumina, with the respective orbital contributions. The partial DOS are obtained projecting the electron wave functions onto atomic-like orbitals, and integrating them around atom-centered spheres. For the spheres radii we have used the Shannon's ionic radii[30] $r^i_O=1.21$ Å and $r^i_{Al}=0.675$ Å, multiplied by a factor $\alpha=1.23173$, to equal the volume of the atomic spheres to the volume of the primitive cell. This shows that there are two groups of valence bands. The lowest one is formed from O $2s$ levels, while the top one is formed from O $2p$. The conduction band presents contributions from all O and Al levels. The Al contribution to the DOS in the valence band is very weak. The absolute values of the partial DOS are strongly dependent on the atomic radii, which have a certain degree of arbitrariness.[47] If the covalent radii are used instead of the ionic radii, the Al partial DOS increases by nearly a factor of 5, but it remains as a minor contribution to the total DOS. Also, its shape remains unchanged inside the valence bands, allowing one to draw qualitative conclusions. As Fig. 4 shows, the upper valence band produces two overlapping peaks in the DOS, which have different Al contributions. The lower energy peak is related to Al $2s$ levels, while the higher energy peak is related to Al $2p$ levels.

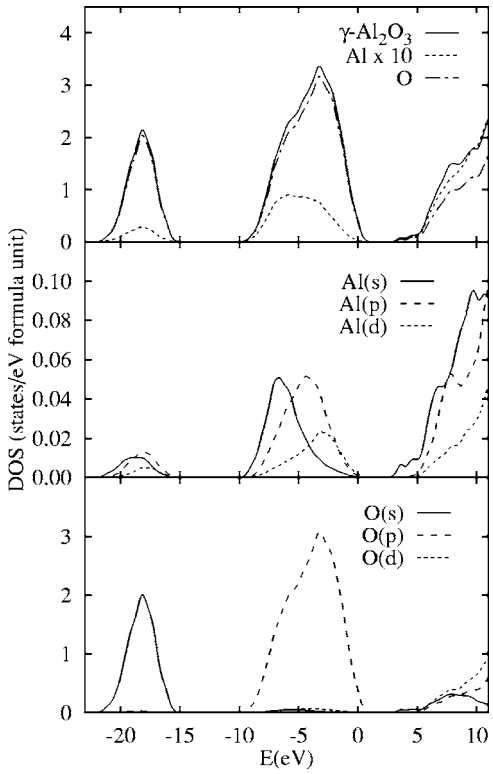

FIG. 4. The total and partial density of states of γ-Al_2O_3 (nonspinel model $Fd\bar{3}m$ of Ref. 19). A Fermi broadening of 0.2 eV was used.

The partial DOS of the spinel models shows the same features as the nonspinel models. Our result agrees with a recent calculation made within the full-potential linear muffin-tin-orbital method[16] performed for the γ-Al_2O_3 spinel structure of Ref. 6. For that structure we obtain a fundamental band gap of 3.960 eV (i.e., 0.244 eV lower than for the relaxed structure). Apart from a uniform shift of the conduction bands (not significant for a DFT calculation), the remaining differences between the band diagrams are of minor character, and the DOS are similar. The DOS of γ-alumina is similar to the DOS of other phases of alumina. Table II shows a comparison of the bandwidths and band gaps for several phases. The most relevant difference among the phases is the fundamental band gap, which is smaller for the phase γ than for the phases α and κ.

Figure 5 shows the band structure for the spinel model. It displays a direct fundamental bandgap of 4.204 eV at the point Γ. The valence bands are distributed in two groups in the ranges $(-20\text{ eV}, -16\text{ eV})$ and $(-9\text{ eV}, 0\text{ eV})$. As suggested by the partial DOS analysis, the first group is formed from the O $2s$ atomic levels, and the second one from the O $2p$ atomic levels. The valence bands are quite flat in the directions Γ-A, H-K, M-L, while the lowest conduction bands are not flat. This is consistent with the smooth edge obtained in Ref. 16 for the imaginary part of the dielectric function.

The band structure of the nonspinel model shows little additional information and is not shown. It is worth while to note that, similarly to the spinel structure, the lowest conduc-

TABLE II. The comparison of bandgaps and widths in several phases of alumina. The results whose source is not indicated correspond to this work.

	γ	κ	α
Width O 2*p*	8.4[b] (LDA)	8 (Ref. 31)	7.2 (Ref. 16)
	8.2[b] (GGA)		8[a] (Ref. 32)
	8.5[b] (Ref. 16)		9.2–9.5[a] (Ref. 33)
	9.0[c] (GGA)		
Width O 2*s*	3.8[b] (LDA)	4 (Ref. 31)	3 (Ref. 16)
	3.9[b] (Ref. 16)		6[a] (Ref. 34)
	3.5[b] (GGA)		
	5.1[c] (GGA)		
Gap	7.9[b] (LDA)	8 (Ref. 31)	8.8 (Ref. 16)
(O 2*s*-O 2*p*)	8.4[b] (GGA)		
	8.0[b] (Ref. 16)		
	7.1[c] (GGA)		
Gap	4.2[b] (LDA)	5.4 (Ref. 31)	6.6 (Ref. 16 and 31)
(valence-	3.8[b] (GGA)		8.8[a] (Ref. 35)
conduction)	3.9[b] (Ref. 16)		
	4.0[b] (Ref. 10)		
	3.5[c] (GGA)		
	3.6[c],[d] (GGA)		
	7.0[a] (Ref. 36)		

[a]Experiment.
[b]Spinel model of γ-alumina.
[c]Nonspinel $Fd\bar{3}m$ model of γ-alumina.
[d]Test calculation using the code ν-ESPRESSO (Ref. 37) and the GGA functional of Perdew, Burke, and Ernzerhof (Ref. 38).

tion band is isolated (although folded and split, because the unit cell is four times larger) from the higher bands.

Figure 6 shows the valence electron density and the ELF in planes containing Al-O bonds, for the case of tetrahedral (left) and octahedral (right) Al coordination. The ELF is a measure of the electron localization in space and helps to visualize the shell structure of atoms and solids. It is defined in terms of the ratio of the excess of kinetic energy due to the Pauli exclusion principle to the Thomas-Fermi kinetic energy density. By definition, ELF values range between 0 and 1. An ELF value close to 1 at a given point indicates a high degree of localization of the electrons at that point. For the homogeneous electron gas, which is used as a reference system in its definition, the ELF is equal to 0.5. Covalent bonds and electron lone pairs in crystals are revealed by local maxima of the ELF.[39,40] Figure 6 shows that most of the charge is distributed around O nuclei. The right panel of Fig. 6 shows the vacancy $V1$ (see the Appendix), where the charge depletion is as large as around the Al atom. The fact that the valence charge density is so small around the Al cations helps to explain why the total energy is so indifferent to the position of the occupied sites and why the structure is so disordered regarding the Al positions. The plots of the electron density and the ELF show that O anions occupy most of the volume, while Al cations are confined to the interstitial positions. The plots of the density difference show a net electronic density transfer towards oxygen and a polarization of the oxygen electronic cloud towards the Al cations. The ELF patterns show weak maxima in the direction of the Al-O bonds, which can be interpreted as a weak partial covalency. In contrast, there is no sign of covalent bonding between O atoms. We have also found this feature in α- and amorphous alumina. For comparison, we also calculated the ELF and the charge density difference for MgO. While the charge density difference also shows maxima in the region of the Mg-O bond, no maxima of the ELF is found.

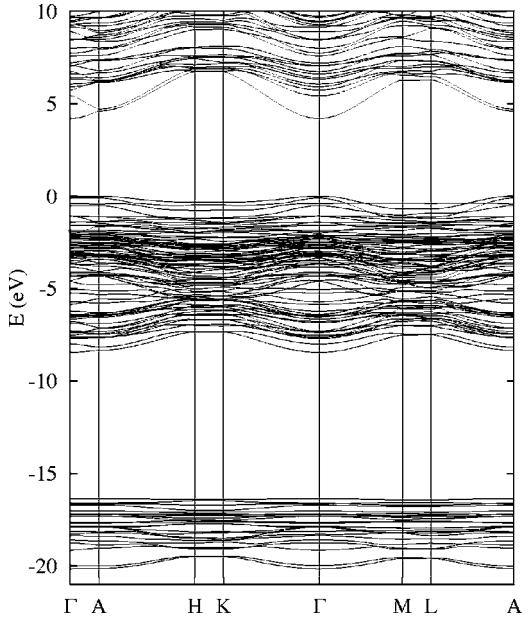

FIG. 5. The band structure of γ-Al_2O_3 (spinel model, LDA). The fractional coordinates of the high symmetry points of the first Brillouin zone are $\Gamma=(0,0,0)$, $A=(0,0,\frac{1}{2})$, $H=(-\frac{1}{3},\frac{2}{3},\frac{1}{2})$, $K=(-\frac{1}{3},\frac{2}{3},0)$, $M=(0,\frac{1}{2},0)$, and $L=(0,\frac{1}{2},\frac{1}{2})$.

Quantitative insight of the ionicity can be obtained analyzing the ionic charge. Following Ruberto *et al.*,[41] we calculate atomic charges integrating the DFT charge density in the Voronoi cell of each atom. By definition, a point $\mathbf{r}$ belongs to the Voronoi cell of atom i if for all atoms j (j running over the nearest neighbors of atom i)

$$\frac{|\mathbf{r}-\mathbf{R}_i|}{b_i} < \frac{|\mathbf{r}-\mathbf{R}_j|}{b_j}, \tag{1}$$

where $\mathbf{R}_{i(j)}$ and $b_{i(j)}$ stand for the position and ionic radius[30] of atom $i(j)$ (we use $b_{Al}=0.675$ Å and $b_O=1.24$ Å). Table III shows the charges calculated for different phases of alumina.

Notice that the calculated ionic charges depend strongly on the assumed atomic radii rather than on the displacement of the electronic cloud due to the bond formation. This is evident looking at the part (b) of Table III, which shows the charges calculated from the (non-self-consistent) superposition of atomic charges. The non-self-consistent charges are close to the self-consistent ones, and far from the null values corresponding to isolated atoms. The difference between the self-consistent and non-self-consistent charges is a measure of the charge transfer and the polarity of the bonds. Part (c)

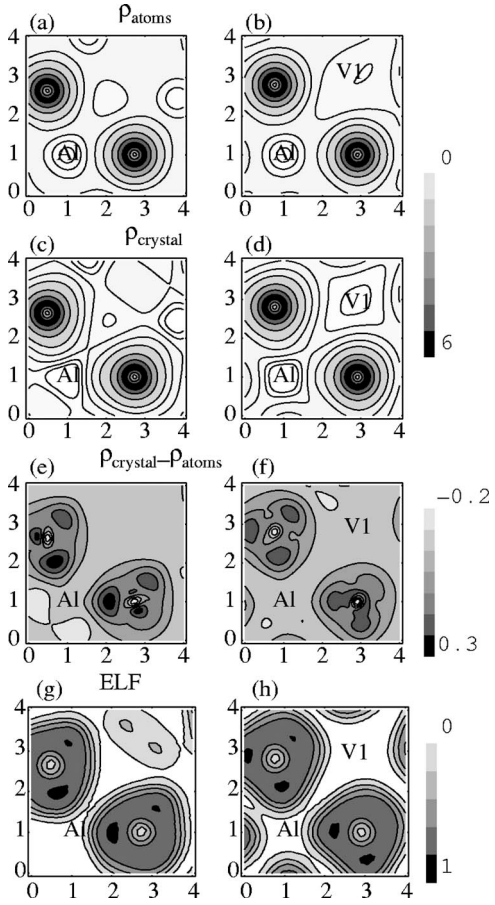

FIG. 6. The plot of the valence electron density and the ELF in two planes containing an Al-O bond: (a,b) superposition of the atomic densities, (c,d) crystal self-consistent density, (e,f) difference between the selfconsistent density and the superposition of atomic densities, and (g,h) electron localization function. Left: plane containing a tetrahedral Al and two O. Right: plane containing an octahedral Al, two O, and a vacancy V1. The contour lines are set to ρ=0.05, 0.10, 0.20, 0.40, 0.8, 2.0, 4.0, and 6 Å^{-3} in (a–d), $\Delta\rho$ =−0.2, −0.1, 0.0, 0.1, 0.2, and 0.3 in (e,f), and ELF=0.17, 0.34, 0.51, 0.68, 0.85 in (g,h).

of Table III shows this difference between crystal and atomic charges, i.e., the charge transfer. It shows that the charge transfer from Al to O is similar in the α and γ phases, independently of the structural model used for γ. The charge transfer for tetrahedral Al(t), absent in α, is slightly smaller than for octahedral Al(o). There is a small dependence of the magnitude of the charge with the exchange-correlation potential and the use of PAW or USPP. However, the trend and the magnitude of the charge transfer is very similar in all the methods. Note that we have employed a single value of the radius of the Al cations, that of octahedrally coordinated Al. This was done to guarantee a fair comparison with α-alumina, which has only octahedral Al. If the tabulated radius[30] 0.53 Å is used for tetrahedral Al(t), keeping 0.675 Å for Al(o), then the calculated ionic charges of Al(t) and O will have higher absolute values. However, in this case the charge transferred to O atoms turns out to be smaller: ~0.05–0.07, compared to the value 0.076–0.086 when only the octahedral radius is used. This illustrates the fact that the

TABLE III. The ionic charges (in units of the proton charge) in α- and γ-alumina according to the partition of the space in Voronoi cells. For the definition of the Voronoi cells we use Shannon radii: 0.675 Å for Al and 1.24 Å for O. Tetrahedral Al(t) and octahedral Al(o) are compared. For the nonspinel γ-alumina the $Fd\bar{3}m$ model of Paglia *et al.* is used.

Material	Method	Al(t)	Al(o)	O
(a) Crystal (self-consistent) charges				
α	LDA-USPP	···	2.80	−1.87
	GGA-PAW	···	2.78	−1.86
	LDA-PAW	···	2.78	−1.86
γ (spinel)	LDA-USPP	2.82	2.80	−1.87
	LDA-PAW	2.79	2.78	−1.86
	GGA-PAW	2.79	2.78	−1.86
γ (nonspinel)	LDA-USPP	2.82	2.80	−1.87
	GGA-PAW	2.80	2.79	−1.86
(b) Atomic (non-self-consistent) charges				
α	LDA-USPP	···	2.67	−1.78
	GGA-PAW	···	2.67	−1.78
	LDA-PAW	···	2.66	−1.77
γ (spinel)	LDA-USPP	2.70	2.68	−1.79
	GGA-PAW	2.68	2.66	−1.78
γ (nonspinel)	LDA-USPP	2.70	2.67	−1.79
	GGA-PAW	2.69	2.67	−1.78
(c) Transferred charges				
α	LDA-USPP	···	0.13	−0.086
	GGA-PAW	···	0.12	−0.079
	LDA-PAW	···	0.12	−0.078
γ (spinel)	LDA-USPP	0.12	0.13	−0.084
	GGA-PAW	0.11	0.12	−0.077
γ (nonspinel)	LDA-USPP	0.12	0.13	−0.084
	GGA-PAW	0.11	0.12	−0.076

movement of the electronic cloud is not uniform (as evidenced in Fig. 6) and the amount of charge transferred depends on the location of the assumed boundaries between the atoms. To have an external reference, let us say that the charge transfer in NaCl calculated by this method is 0.12 electron charges, and 0.20 for MgO.

IV. CONCLUSIONS

Recent experimental and computational results allow us a satisfactory understanding of the structure of γ-alumina. The new structural models obtained by computational methods are consistent with neutron diffraction patterns. A crucial role in the agreement with the diffraction patterns is played by the occupation of nonspinel positions by a fraction of the Al cations. However, the calculated total energy of the theoretical nonspinel structure is not lower than for the spinel structure. The energy difference is certainly small (~5 meV/atom), and this could be due to systematic errors

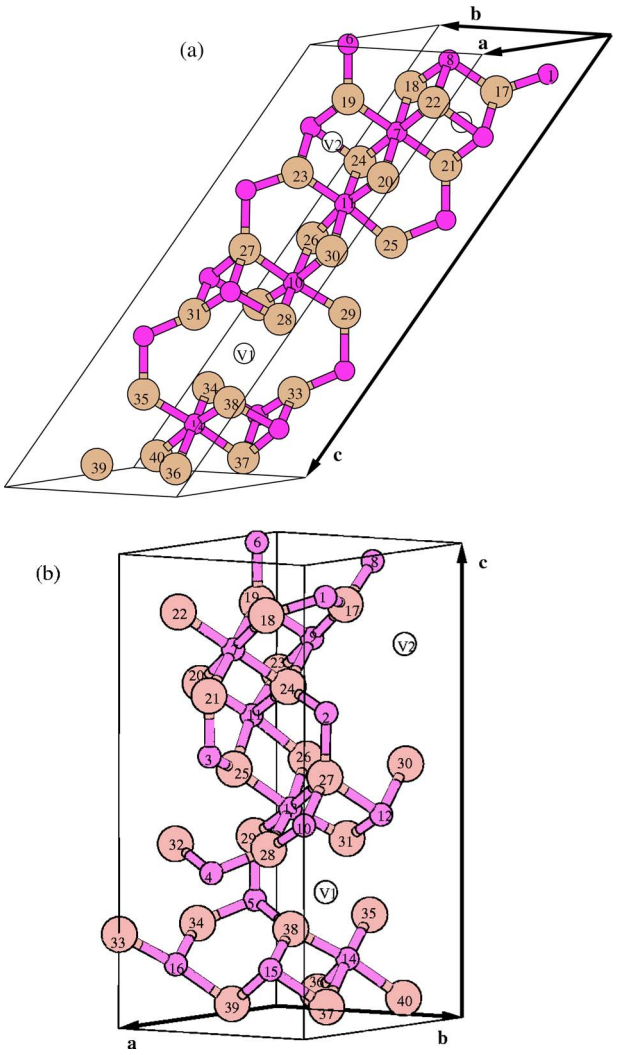

FIG. 7. (Color online) The unit cell of the optimized structure for γ-Al_2O_3. (a) The primitive lattice vectors are $\mathbf{a}=a(0,\frac{1}{2},\frac{1}{2})$, $\mathbf{b}=a(\frac{1}{2},0,\frac{1}{2})$, $\mathbf{c}=a(\frac{3}{2},\frac{3}{2},0)$. (b) Compact unit cell obtained by a change of basis $\mathbf{a}'=-\mathbf{b}$, $\mathbf{b}'=\mathbf{b}-\mathbf{a}$, $\mathbf{c}'=\mathbf{a}+\mathbf{b}-\mathbf{c}$, followed by a relaxation of both the cell and the ionic positions. Big circles represent O atoms, small circles represent Al atoms, and the white circles show the positions of the two Al vacancies in 16*d* positions. Generated with XCRYSDEN (Refs. 42 and 43).

inherent to the LDA and GGA or the use of pseudopotentials or PAW. Also, the zero-point energy or entropy terms in the free energy at the temperature of synthesis could make the difference favorable to the nonspinel structures.

We have studied in detail the electronic structure for the most recent theoretical structural models. The bandgap is smaller than for α- and κ-alumina, confirming previous calculations with other methods. The charge transfer between Al and O ions is similar to that of α-alumina. This suggests that the reduction of the band gap is due to the structural disorder of the γ phase, and not to differences in ionicity. The partial DOS analysis shows that the valence band is dominated by oxygen levels, with the O 2*s* and O 2*p* contributions distributed in well-separated bands. A graphical description of the spatial features of the electronic structure has been presented by means of the electronic density and the ELF. This information shows that the valence charge density at Al sites is almost indifferent to the fact that the site is occupied or not (vacancy). This helps to understand why the Al sublattice is so disordered. The ELF shows that, despite the ionic character of the Al-O bonds, there are local maxima in the bond region. This indicates a certain degree of covalency, which is common with other phases of alumina, and is not seen in more ionic solids, such as MgO and NaCl.

TABLE IV. The atomic fractional coordinates of the LDA relaxed structure in the γ-Al_2O_3. The numbers assigned to the atoms and the lattice vectors correspond to Fig. 7(b).

a=5.6061 Å, b=5.5699 Å, c=13.482 Å
α=89.4°, β=90.0°, γ=120.2°

Al	x	y	z	O	x	y	z
1	0.6639	0.8279	0.9135	17	0.3217	0.6438	0.8774
2	0.6693	0.8387	0.6692	18	0.8219	0.6437	0.8774
3	0.9905	0.4810	0.5841	19	0.3453	0.1906	0.8707
4	0.9997	0.4994	0.3388	20	0.5113	0.0228	0.7052
5	0.3337	0.1674	0.2438	21	0.9879	0.4760	0.7119
6	0.3428	0.1856	0.9985	22	0.8438	0.1876	0.8751
7	0.6666	0.3333	0.7913	23	0.0115	0.0228	0.7052
8	0.0157	0.5315	0.9515	24	0.4895	0.4790	0.7076
9	0.1666	0.3333	0.7913	25	0.6345	0.3114	0.5369
10	0.9700	0.9910	0.4510	26	0.1769	0.3115	0.5369
11	0.3175	0.1351	0.6312	27	0.6626	0.8254	0.5333
12	0.5011	0.9910	0.4510	28	0.8301	0.6637	0.3847
13	0.5001	0.5003	0.4519	29	0.3305	0.1610	0.3784
14	0.3434	0.6757	0.1317	30	0.1714	0.8429	0.5386
15	0.8323	0.6757	0.1317	31	0.3337	0.6638	0.3847
16	0.8332	0.1664	0.1308	32	0.8308	0.1616	0.3848
				33	0.9997	0.0030	0.1980
				34	0.5034	0.0030	0.1980
				35	0.0029	0.5059	0.2043
				36	0.1565	0.3552	0.0458
				37	0.6706	0.8413	0.0494
				38	0.5026	0.5051	0.1979
				39	0.6988	0.3552	0.0458
				40	0.1618	0.8237	0.0441

ACKNOWLEDGMENTS

This work has been supported by FONDECYT (Chile) Grant Nos. 7030083 and 1030063. E.M.-P. acknowledges the University of Santiago de Chile and the Abdus Salam ICTP, where part of this work was done. G.G. acknowledges the Núcleo Materia Condensada-Iniciativa Científica Milenio P02-054-F. We also thank Henry Pinto and Gianluca Paglia for providing their optimized theoretical structures, Walter Orellana for a critical reading of the manuscript, and G. Paglia for a stimulating discussion of it.

APPENDIX A: OPTIMIZED STRUCTURE OF THE SPINEL MODEL

Figure 7(a) shows the unit cell of the structure determined in Ref. 6. The primitive lattice vectors $\mathbf{a},\mathbf{b},\mathbf{c}$ are shown in the figure. Notice that the vectors $\mathbf{a}$, $\mathbf{b}$, and $\frac{1}{3}\mathbf{c}$ correspond to the primitive vectors of the original fcc lattice. Figure 7(b) shows the structure of the primitive cell used in the present calculation. This unit cell corresponds to a redefinition of the former primitive vectors: $\mathbf{a}'=-\mathbf{b}$, $\mathbf{b}'=\mathbf{b}-\mathbf{a}$, $\mathbf{c}'=\mathbf{a}+\mathbf{b}-\mathbf{c}$. Now, we have a unit cell which presents the advantage that the c axis is perpendicular to the O planes. It also reveals the layered structure as composed of alternating planes of Al and O atoms stacked in the $\mathbf{c}$ direction.

The structure obtained before relaxation of the cell shape[6] has a shear stress (ZX component) of approximately 30 kbar, which can only be eliminated at the price of reducing the symmetry of the lattice. The shear stress is present with any of the two unit cells. We performed a full relaxation of the cell and the ionic positions in such a way that the remaining stress components were smaller than 0.05 kbar, and the forces on the ions were smaller than 0.005 eV/Å (i.e., 8×10^{-12} N). After that, the obtained lattice parameters were $a=5.6061$ Å, $b=5.5699$ Å, and $c=13.482$ Å with angles $\alpha=89.4°$, $\beta=90.0°$, and $\gamma=120.2°$, resulting in a kind of pseudo-hexagonal lattice. This distortion of the lattice represents a change of the conventional cubic cell from a perfect cube with the theoretical values of side lengths $a_0=b_0=c_0=7.864$ Å and angles $\alpha_0=\beta_0=\gamma_0=90°$ (conventional spinel-type $Al_{21(1/3)}O_{32}$, to a distorted cube with side lengths $\tilde{a}_0=\tilde{c}_0=7.848$ Å, $\tilde{b}_0=7.877$ Å, and angles $\tilde{\alpha}_0=89.8°$, $\tilde{\beta}_0=88.8°$, and $\tilde{\gamma}_0=89.8°$. The fractional atomic coordinates' change is less than 0.1% after the relaxation. The final structure obtained is summarized in Table IV.

*Also at Condensed Matter Theory Group, Uppsala University, Sweden.

[1] K. Wefers and C. Misra, *Tech. Rep.* 19, Alcoa Laboratories (1987), revised.

[2] S. Wang, A. Y. Borisevich, S. N. Rashkeev, M. V. Glazoff, K. Sohlberg, S. J. Pennycook, and S. Pantelides, Nat. Mater. **3**, 143 (2004).

[3] G. Paglia, C. E. Buckley, A. L. Rohl, B. A. Hunter, R. D. Hart, J. V. Hanna, and L. T. Byrne, Phys. Rev. B **68**, 144110 (2003).

[4] E. J. W. Verway, Z. Kristallogr. **91**, 65 (1935).

[5] R.-S. Zhou and R. L. Snyder, Acta Crystallogr., Sect. B: Struct. Sci. **47**, 617 (1991).

[6] G. Gutiérrez, A. Taga, and B. Johansson, Phys. Rev. B **65**, 012101 (2002).

[7] G. Paglia, C. E. Buckley, A. L. Rohl, R. D. Hart, K. Winter, A. J. Studer, B. A. Hunter, and J. V. Hanna, Chem. Mater. **16**, 220 (2004).

[8] S.-H. Cai, S. N. Rashkeev, S. T. Pantelides, and K. Sohlberg, Phys. Rev. Lett. **89**, 235501 (2002).

[9] S.-H. Cai, S. N. Rashkeev, S. T. Pantelides, and K. Sohlberg, Phys. Rev. B **67**, 224104 (2003).

[10] H. P. Pinto, R. M. Nieminen, and S. D. Elliott, Phys. Rev. B **70**, 125402 (2004).

[11] K. Sohlberg, S. J. Pennycook, and S. T. Pantelides, J. Am. Chem. Soc. **121**, 7493 (1999).

[12] K. Sohlberg, S. J. Pennycook, and S. T. Pantelides, Chem. Eng. Commun. **181**, 107 (2000).

[13] L. J. Alvarez, J. Fernández, M. J. Capitán, and J. A. Odriozola, Chem. Phys. Lett. **192**, 463 (1993).

[14] S.-D. Mo, Y.-N. Xu, and W.-Y. Ching, J. Am. Ceram. Soc. **80**, 1193 (1997).

[15] F. H. Streitz and J. W. Mintmire, Phys. Rev. B **60**, 773 (1999).

[16] R. Ahuja, J. M. Osorio-Guillen, J. Souza de Almeida, B. Holm, W. Y. Ching, and B. Johansson, J. Phys.: Condens. Matter **16**, 2891 (2004).

[17] C. Wolverton and K. C. Hass, Phys. Rev. B **63**, 024102 (2001).

[18] G. Paglia, C. E. Buckley, A. L. Rohl, R. D. Hart, F. Jones, C. F. Maitland, and J. Connolly, Chem. Mater. **16**, 1914 (2004).

[19] G. Paglia, Ph.D. thesis, Curtin University of Technology (2004), available at http://adt.curtin.edu.au/theses/available/adt-WCU20040621.123301/; G. Paglia, A. L. Rohl, C. E. Buckley, and J. D. Gale, Phys. Rev. B (to be published).

[20] P. Hohenberg and W. Kohn, Phys. Rev. **136**, B864 (1964).

[21] W. Krauss and G. Nolze, PowderCell for Windows, version 2.4, Federal Institute for Material Research and Testing, Rudower Chausee 5, 12489 Berlin, Germany.

[22] A. D. Becke and K. E. Edgecombe, J. Chem. Phys. **92**, 5397 (1990).

[23] A. Savin, O. Jepsen, J. Flad, O. Andersen, H. Preuss, and H. G. von Schnering, Angew. Chem., Int. Ed. Engl. **31**, 187 (1992).

[24] M. Kohout and A. Savin, Int. J. Quantum Chem. **60**, 875 (1996).

[25] G. Kresse and J. Hafner, Phys. Rev. B **47**, R558 (1993).

[26] G. Kresse and J. Hafner, Phys. Rev. B **49**, 14251 (1994).

[27] G. Kresse and J. Furthmüller, Comput. Mater. Sci. **6**, 15 (1996).

[28] G. Kresse and J. Furthmüller, Phys. Rev. B **54**, 11169 (1996).

[29] J. P. Perdew and A. Zunger, Phys. Rev. B **23**, 5048 (1981).

[30] R. D. Shannon, Acta Crystallogr., Sect. A: Cryst. Phys., Diffr., Theor. Gen. Crystallogr. **32**, 751 (1976).

[31] Y. Yourdshahyan, C. Ruberto, L. Bengtsson, and B. I. Lundqvist, Phys. Rev. B **56**, 8553 (1997).

[32] G. Dräger and J. A. Leiro, Phys. Rev. B **41**, 12919 (1990).

[33] W. L. O'Brien, J. Jia, Q.-Y. Dong, T. A. Callcott, K. E. Miyano, D. L. Ederer, D. R. Mueller, and C.-C. Kao, Phys. Rev. B **47**, 140 (1993).

[34] A. Balzaroti and A. Bianco, Phys. Status Solidi B **76**, 689 (1976).

[35] R. H. French, J. Am. Ceram. Soc. **73**, 477 (1990).

[36] B. Ealet, M. H. Elyakhloufi, E. Gillet, and M. Ricci, Thin Solid Films **250**, 92 (1994).

[37] S. Baroni, A. D. Corso, S. de Gironcoli, P. Giannozzi, C. Cavazzoni, G. Ballabio, S. Scandolo, G. Chiarotti, P. Focher, A. Pasquarello, K. Laasonen, A. Trave, R. Car, N. Marzari, and A. Kokalj, ν-ESPRESSO *package* (2005), http://www.pwscf.org/.

[38] J. P. Perdew, K. Burke, and M. Ernzerhof, Phys. Rev. Lett. **77**, 3865 (1996).

[39] U. Haussermann, S. Wengert, P. Hofmann, A. Savin, O. Jepsen, and R. Nesper, Angew. Chem., Int. Ed. Engl. **33**, 2069 (1994).
[40] U. Haussermann, S. Wengert, and R. Nesper, Angew. Chem., Int. Ed. Engl. **33**, 2073 (1994).
[41] C. Ruberto, Y. Yourdshahyan, and B. I. Lundqvist, Phys. Rev. B **67**, 195412 (2003).
[42] A. Kokalj, J. Mol. Graphics Modell. **17**, 176 (1999).
[43] A. Kokalj and M. Causa, in *Proceedings of High Performance Graphics Systems and Applications European Workshop*, Bologna, 2000, pp. 51–54.
[44] R. F. W. Bader, *Atoms in Molecules: A Quantum Theory* (Clarendon Press, Oxford, 1990).
[45] The spinel structure also has lower energy in the LDA. We also made a test calculation with the package ν-ESPRESSO (Ref. 37), confirming that the spinel structure has lower energy.
[46] This distortion is within the experimental range. However, it is also within the accuracy of DFT methods.
[47] Shannon's ionic radii are based on geometrical ideas and the nuclear arrangement, rather than on electronic structure. On the other hand, the topological properties of the total electronic charge density and the ELF provide well-defined (although more complex) schemes for partition of the space in (nonspherical) atomic and electronic domains (Refs. 40 and 44).